Title

Directly Functionalized Cucurbit[7]uril as a Biosensor for the Selective Detection of Protein Interactions by 129Xe hyperCEST NMR

Journal

Chemistry - A European Journal, 25(24)

ISSN

0947-6539

Authors

Truxal, Ashley E
Cao, Liping
Isaacs, Lyle
et al.

Publication Date

2019-04-26

DOI

10.1002/chem.201900610

Peer reviewed

HHS Public Access

Author manuscript

Chemistry. Author manuscript; available in PMC 2020 April 26.

Published in final edited form as:

Chemistry. 2019 April 26; 25(24): 6108–6112. doi:10.1002/chem.201900610.

Directly functionalized cucurbit[7]uril as a biosensor for the selective detection of protein interactions by ^{129}Xe hyperCEST NMR

Ashley E. Truxal[1], **Dr. Liping Cao**[2], **Prof. Dr. Lyle Isaacs**[3], **Prof. Dr. David E. Wemmer**[1], and **Prof. Dr. Alexander Pines**[1]

[1]University of California Berkeley, Berkeley, CA, USA.

[2]Northwest University, College of Chemistry and Materials Science, Xi'an, China.

[3]University of Maryland, Department of Chemistry and Biochemistry, College Park, MD, USA.

Abstract

Advancement of hyperpolarized ^{129}Xe MRI technology toward clinical settings demonstrates the considerable interest in this modality for diagnostic imaging. The number of contrast agents, termed biosensors, for ^{129}Xe MRI that respond to specific biological targets, has grown and diversified. Directly functionalized xenon-carrying macrocycles, such as the large family of cryptophane-based biosensors, are good for localization-based imaging and provide contrast before and after binding events occur. Non-covalently functionalized constructs, such as cucurbituril- and cyclodextrin-based biosensors, benefit from commercial availability and optimal exchange dynamics for CEST imaging. In this work, we report the first directly functionalized cucurbituril used as a xenon biosensor. Biotinylated cucurbit[7]uril (btCB7) gives rise to a ^{129}Xe hyperCEST response at the unusual shift of 28 ppm when bound to its protein target with substantial CEST contrast. We posit that the observed chemical shift is due to the deformation of btCB7 upon binding to avidin, caused by proximity to the protein surface. Conformational searches and molecular dynamics (MD) simulations support this hypothesis. This construct combines the strengths of both families of biosensors, enables a multitude of biological targets through avidin conjugation, and demonstrates the advantages of functionalized cucurbituril-based biosensors.

Graphical Abstract

Specific binding of a biotinylated cucurbit[7]uril to avidin yields a 129Xe chemical shift that is far removed from any other 129Xe biosensor to date due to strong cage interactions with the protein surface. This result widens the breadth of biological targets of 129Xe MRI via avidin conjugation.

dewemmer@berkeley.edu.

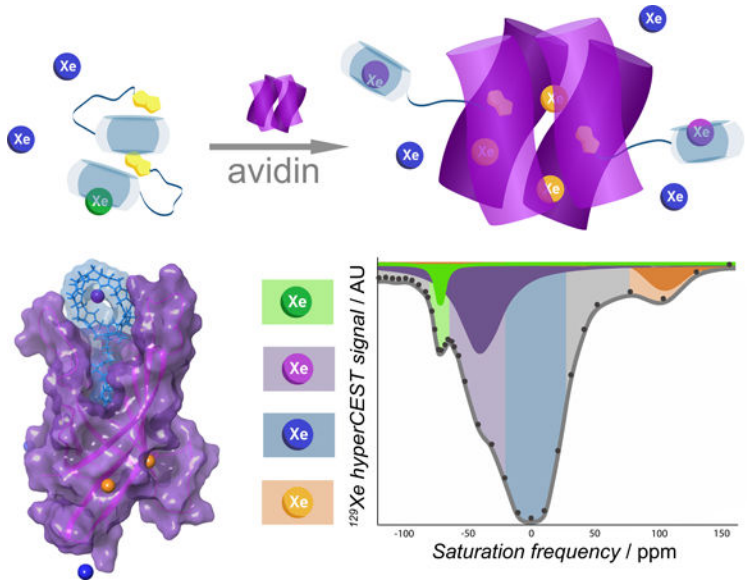

Keywords

biosensors; host-guest systems; hyperpolarization; imaging agents; ^{129}Xe NMR

Hyperpolarized imaging agents are particularly attractive for quantitative and targeted contrast magnetic resonance imaging (MRI) applications because their high sensitivity, low background signal, and long relaxation times enable direct visualization of physiologic processes or specific molecular targets. While hyperpolarized ^{3}He gas and ^{13}C- and ^{15}N-labeled agents have continued to demonstrate their potential for clinical application, hyperpolarized ^{129}Xe gas remains at the forefront for targeted molecular imaging.[1] Xenon is appealing as a MRI imaging agent because it is inert and exogenous, has good aqueous solubility, and has a high polarizability that makes it very sensitive to its local chemical environment.[2–4] ^{129}Xe nuclei can be hyperpolarized by spin exchange optical pumping to increase signal by 4–5 orders of magnitude compared to thermal polarization, which enables imaging at modest dissolved xenon concentrations.[5] Hyperpolarized ^{129}Xe MRI was first used in lung imaging, and more recently for *in vivo* detection and characterization of asthma, chronic obstructive pulmonary disease, and fibrotic lung diseases[2–4,6]. Xenon has also been used to probe structure and dynamics of hydrophobic regions in proteins, and more recently for targeted molecular imaging.[7]

The advent of macromolecular hosts with which xenon atoms transiently associate has enabled selective, localized detection of a diverse range of biological targets. Xenon atoms exchange in and out of the hosts and can act as a reporter of the hosts' chemical environment through changes in ^{129}Xe chemical shift or relaxation. When hosts interact with a specific biological or chemical target, they give rise to distinct ^{129}Xe NMR signals.[1]

Chemical exchange saturation transfer techniques can be applied to hyperpolarized xenon (^{129}Xe hyperCEST), exploiting the exchange of thousands of xenon atoms with a single host within a T_1 relaxation period. When the signal from xenon residing in the host is saturated

with an RF pulse, a reduction in the large signal arising from xenon dissolved in bulk solution is observed. This provides an indirect but ultrasensitive detection scheme that has brought detection limits of xenon hosts to nano- and picomolar scales.[6]

These xenon-host ensembles, termed biosensors, currently come in two major classes: supramolecular compounds such as conjugates of cryptophanes, cyclodextrins, pillar[5]arenes, cucurbiturils and metal-organic frameworks; and larger compartmental carriers including viral capsids, gas vesicles and liposomes.[8–13] The ever-expanding array of xenon biosensors has been applied to the selective detection of a variety of binding events involving metal ions, receptors on cell surfaces, transmembrane proteins, enzymes, biothiols, and reporting on microenvironments indicative of tumors, such as abnormal pH, specific ionic milieus or oxidation.[9,10,13–24]

Cucurbit[n]urils (CBns) comprise a class of hosts for ^{129}Xe hyperCEST applications, which are useful because of their commercial availability and favorable xenon exchange kinetics.[25] CBns are donut-shaped molecules comprised of *n* glycoluril units linked by methylene bridges (Fig. 1a, CB7 shown) that can form dynamic host-guest complexes with a variety of moieties. As xenon biosensors, derivatives of the six-membered structure, CB6, have been most frequently used, though CB7 has recently shown promise as a faster-exchanging, alternative host.[21] Exchange rates of these cages with xenon are low enough to be within the slow-to-intermediate exchange regime, yielding a distinct resonance for xenon residing in CB6 or CB7, but large enough to gain signal enhancement via hyperCEST. However, CB6 has poor aqueous solubility compared to CB7, and both can bind nonspecific guests that exclude xenon.[26] Further, the difficulty of functionalizing CBns has restricted CBn-based biosensors to indirect detection methods, those in which the sensors remain inaccessible to xenon until some specific event “unlocks” them. The CBn moieties are then identical when active, meaning all such sensors will have the same chemical shift upon interaction with their target.[27–29]

Recently, CBns have been explored as drug carriers that improve chemical stability and solubility of their drug payload.[26,30,31] Further, CB7 has shown utility for controlled release of drugs in cancerous cells.[32] Cao *et al.* reported synthesis of a directly biotinylated CB7 (btCB7, Fig. 1a) as a carrier for anti-cancer drugs to murine lymphocytic leukemia (L1210FR) cancer cells, which overexpress biotin receptors.[33] The drug-btCB7 complexes demonstrated improved targeting specificity and cytotoxicity to L1210FR cells, while preserving healthy tissue and preventing side effects associated with non-selective toxicity. We investigated btCB7 as a potential xenon biosensor for the small protein avidin, for which biotin has a very high affinity ($K_a \approx 10^{15}$ M^{-1}), with the aim of combining the target specificity conferred by directly functionalized xenon biosensors with the optimal hyperCEST characteristics of CBns. Specific detection of avidin makes possible biosensor customization, as avidin can be conjugated to other proteins and/or with other detection agents.[34]

As a first step we examined whether biotinylation affected the observable ^{129}Xe hyperCEST signal for xenon inside btCB7 (Xe@btCB7), Figure 1. As a control we first measured the hyperCEST response from unmodified CB7, Figure 1b, which is very similar to that

reported previously by Schnurr *et al*.[21] For Xe@btCB7 the response is again at −68 ppm, but is significantly weaker than that for unmodified CB7 (Fig.1b). Both hyperCEST signals are meager compared to typical CB6 responses at the same concentration. CB6 responses observed by others are fairly broad, which is attributed to facile exchange from the central cavity (diameter 5.8Å). For CB7, with a larger diameter of 7.3 Å exchange should be even faster, and in that case a much broader Xe@CB7 signal is expected. Additionally the broadening of the water dissolved xenon at 0 ppm is larger than expected given the width and intensity of the bound xenon peak. As such we believe that the peaks at −68 ppm arise from a known, low-population (≈1%) stereoisomer iCB7, in which a single glycouril unit is inverted (Fig. 1c–d).[35] The 'inverted' CBns (iCBns) have a reduced internal cavity size relative to the normal CBn, ≈ 5.5Å diameter for iCB7, and a preference for smaller guests. The smaller cavity explains the presence of weak, relatively sharp, CEST Xe signal from iCB7. We believe that the CB7 bound xenon resonance is too broad to directly detect, but the presence of Xe in CB7 is manifested through broadening of the water dissolved xenon peak.[35]

The Xe@ibtCB7 signal is significantly weaker than that from Xe@iCB7. Given that both structures have the same xenon chemical shift, their internal cavitiy environments are likely equivalent. It is possible that less ibtCB7 was formed during its synthesis than iCB7 during unmodified CB7 synthesis. Yields of the inverted isomer are reported as somewhat variable.[25] Alternately, xenon binding to ibtCB7 could be inhibited by an exclusion complex between ibtCB7 and its own biotin tail or that of another ibtCB7. CBns are known to form such exclusion complexes with short peptides as well as long diammonium alkanes,[36] but our MD simulations showed that the biotinylated tail does not appear to obstruct the CB7 portals (Fig 1c, right). The original report of btCB7 showed that it self-associates as dimers in solution, making the exclusion of xenon by aggregation another potential source of CEST response suppression.[33] MALDI analysis of our samples supports the presence of dimers (Fig. S1), and further MD simulations show that two proximal ibtCB7 molecules quickly form persistent dimers where the biotin tails rest atop one another (Fig. 1d). Avidin binding is strong and disrupts btCB7 dimerization.[23] Both monomeric and dimeric ibtCB7 modeled environments showed transient deformation of the CB7 portion of ibtCB7 around bound xenon atoms. This result is in line with previous work demonstrating the propensity of CB6 for flexing to accommodate guest molecules due to the thermodynamic benefit of freeing high energy water from its inner volume.[37,38]

To evaluate the potential as a biosensor we studied btCB7 bound to avidin. Avidin is a homotetramer of ≈ 68 kD that contains one biotin receptor on each of its four subunits. Samples were made with 0.5 to 2 equivalents of biotin receptors relative to the btCB7, which was maintained at 50 μM. Upon the addition of avidin to samples containing btCB7, we observed four distinct signals as shown in Fig. 1e–f. The Xe@ibtCB7 and water-dissolved xenon signals are seen at −68 ppm and 0 ppm, along with new signals at roughly −40 ppm and 100 ppm. We attribute the response at 100 ppm to the interaction of xenon atoms with avidin directly. In experiments with xenon in solution with only avidin this signal is present (Fig. S2). It is well known that xenon binds to hydrophobic pockets and channel pores in proteins.[4,7,39,40] Recently, binding of xenon to maltose binding protein and TEM β-

lactamase was observed by ^{129}Xe NMR, giving generally similar shifts (60–95 ppm downfield of the dissolved xenon resonance).[41,42]

The substantial response at −40 ppm is assigned to btCB7 bound to avidin (Xe@btCb7-avidin). To verify this we performed a number of controls: there was no signal at −40 ppm for unmodified CB7 in the presence of avidin (Fig. 1e), or for btCB7 in the presence of avidin that was pre-saturated with biotin (Fig. 1f). The assignment of the other CEST signals to other species are shown in Fig. 2a–b. Increasing the avidin concentration yielded a larger signal at −40 ppm, but broadening of the xenon in solvent response caused by chemical exchange (that also affects the hyperCEST spectrum) made direct quantification difficult (Fig S3). We performed Lorentzian fitting of the full spectra, which allowed for the separation and estimation of each population's contribution. This confirmed that the magnitude of the avidin bound btCB7 response increased for increasing amounts of avidin relative to biosensor.

Having identified the signal from btCB7 bound to avidin, we estimated imaging contrast potential by comparing 'on' versus 'off' resonance CEST to the xenon in solvent peak (Fig. 2c). Saturation at the frequency of btCB7 bound to avidin (−40 ppm, 'on') comparted to the control (40 ppm, 'off') generates ≈ 50% CEST difference, which is sufficient to provide significant imaging contrast.

Further verification that the signal at −40 ppm arises from btCB7 was provided by addition of the drug oxaliplatin, known to bind CB7 with high affinity (≈ 10^8 M^{-1}).[33] With drug bound the CB7 cavity is filled, displacing any xenon and preventing rebinding. Consistent with this, addition of oxaliplatin to the btCB7-avidin sample led to complete loss of the signal at −40 ppm. This experiment also supports the assignment of the peak at −68 ppm as arising from iCB7. The smaller cavity from the inverted isomer of the CB7 cannot bind oxaliplatin, and the −68 signal is not affected by addition of the drug, Fig. 3 and S4.

To help understand the avidin bound Xe@btCB7 signal we performed docking and MD simulations on the btCB7-avidin complex in the presence of xenon (Fig 3, top). These simulations showed that btCB7 fits into the biotin binding pocket of monomeric avidin with the CB7 moiety resting snugly between the loops L3,4 and L7,8 in the monomer. Such interactions may slightly occlude the CB7 and slow the xenon exchange such that a broad but clear resonance from it can be observed via CEST. Xenon atoms were also observed in pockets of the avidin (orange), Fig. 3. Simulation trajectories confirmed that the CB7 portion of avidin-bound btCB7 experiences dynamic deformation that is more pronounced than its unbound counterpart (Fig. S5). The short tether between CB7 and biotin appears to hold the CB7 in close proximity to the protein surface. These results support contact-mediated cage deformations as a source of the relatively downfield ^{129}Xe chemical shift for btCB7 bound to avidin, as has been seen for somewhat analogous xenon biosensors.[43–45] The ability to achieve close proximity of these cages to protein targets makes functionalized CB-based biosensors very attractive for imaging applications.

In summary, we have presented the first example of a directly functionalized cucurbituril used for detection of a specific protein target by ^{129}Xe hyperCEST. This work additionally

lays the foundation for detection of many biological target through the use of avidin conjugation (e.g. to targeting antibodies). These observations support the potential for cucurbituril-based xenon biosensors to selectively, sensitively and potentially simultaneously report on multiple pathological markers in a single ^{129}Xe imaging session.

Experimental Section

Sample preparation

btCB7 (Dr. Liping Cao, Isaacs Group, Dept. of Chemistry and Biochemistry, UMD), biotin (Sigma-Aldrich), and avidin from egg white (Sigma-Aldrich, Rockland) were each received as solid powders and dissolved in phosphate-buffered saline solution before use. For avidin titration experiments, the amount of avidin was increased, while the concentration of btCB7 remained constant (50 μM). Ratios were calculated based on number of binding sites per avidin molecule and given equilibrium conditions. MALDI data was acquired from a Bruker microflex LT instrument.

Xenon HyperCEST experiments

Xenon hyperpolarization and delivery was achieved on two xenon polarizer setups and described in detail in the Supporting Information. To acquire ^{29}Xe hyperCEST z-spectra, saturation frequencies are arrayed so any exchange of xenon between bulk water and cages appear as reduction in the dissolved xenon resonance when the saturation frequency matches the frequency corresponding to the caged xenon chemical shift. Each FID in hyperCEST datasets was processed by integrating the area of the FID for each saturation frequency, then dividing by the largest area in the set to normalize. All areas are then plotted versus saturation frequency to yield a z-spectrum. All z-spectra for a given sample were averaged then subjected to fitting by way of a least-squares iterative fit function applied to a simple Lorentzian model.

%CEST effect was determined by comparing ‘on’ resonance saturation at the btCB7-avidin response at 40 ppm with respect to the dissolved xenon response with ‘off’ resonance saturation at the frequency on the opposite side of and equidistant from the dissolved xenon signal, i.e. at 40 ppm.

Computational modeling

BtCB7 structures were built in Maestro (v. 2018–1) and subjected to minimization and conformational searches using the Macromodel conformational search tool with the OPLS-2005 force field. The monomeric avidin structure was obtained from the Protein Database (PDB ID: 2AVI) then run through minimization and Protein Prep Wizard in Maestro. BtCB7 docking on avidin was accomplished by Induced Fit calculations using the OPLS-2005 force field. Molecular dynamics simulations for monomeric, dimerized, and avidin-bound btCB7 were prepared in orthorhombic boxes of 0.15 M NaCl(aq) with Cl^- added to neutralize any charge and applying the SPC solvent model. Xenon atoms were modeled by using the van der Waals radii of I^- atoms and setting their charge to 0. Several iterations of 100 nanosecond trajectories using an NPT ensemble at 293K and 1.013 bar were simulated in Desmond.

Supplementary Material

Refer to Web version on PubMed Central for supplementary material.

Acknowledgements

The authors thank Dr. Leif Schröder and his group at the Leibniz-Forschungsinstitut für Molekulare Pharmakologie for allowing the use of their xenon polarizer setup for this work and for their helpful discussions. The author extends gratitude to Dr. Cynthia Jameson, Dr. Kathleen Durkin and Dr. David Small for their guidance regarding computational modeling, which was funded by NIH grant S10OD023532. LI thanks the NSF (CHE-1404911 and CHE-1807486) for financial support.

References

[1]. Mcmahan ZH, Wigley FM, HHS Public Access, 2015.

[2]. Witte C, Kunth M, Döpfert J, Rossella F, Schröder L, J. Vis. Exp 2012, DOI 10.3791/4268.

[3]. Oros AM, Shah NJ, Phys. Med. Biol 2004, 49, DOI 10.1088/0031-9155/49/20/R01.

[4]. Cherubini A, Bifone A, Prog. Nucl. Magn. Reson. Spectrosc 2003, 42, 1–30.

[5]. Walker TG, Happer W, Rev. Mod. Phys 1997, 69, 629–642.

[6]. Schröder L, Phys. Medica 2013, 29, 3–16.

[7]. Prangé T, Schiltz M, Pernot L, Colloc'h N, Longhi S, Bourguet W, Fourme R, Exploring Hydrophobic Sites in Proteins with Xenon or Krypton, 1998.

[8]. Wang Y, Dmochowski IJ, Acc. Chem. Res 2016, 49, 2179–2187. [PubMed: 27643815]

[9]. Rose HM, Witte C, Rossella F, Klippel S, Freund C, Schroder L, Proc. Natl. Acad. Sci 2014, 111, 11697–11702. [PubMed: 25071165]

[10]. Mari E, Berthault P, Analyst 2017, 142, 3298–3308. [PubMed: 28831479]

[11]. Shapiro MG, Ramirez RM, Sperling LJ, Sun G, Sun J, Pines A, Schaffer DV, Bajaj VS, Nat. Chem 2014, 6, 629–634. [PubMed: 24950334]

[12]. Roukala J, Zhu J, Giri C, Rissanen K, Lantto P, Telkki VV, J. Am. Chem. Soc 2015, 137, 2464–2467. [PubMed: 25671394]

[13]. Guo Q, Zeng Q, Jiang W, Zhang X, Luo Q, Zhang X, Bouchard LS, Liu M, Zhou X, Chem. - A Eur. J 2016, 22, 3967–3970.

[14]. Zhang B, Guo Q, Luo Q, Zhang X, Zeng Q, Zhao L, Yuan Y, Jiang W, Yang Y, Liu M, et al., Chem. Commun 2018, 54, 13654–13657.

[15]. Yuan Y, Guo Q, Yang S, Bouchard L-S, Liu M, Luo Q, Ren L, Zhang B, Zhou X, Jiang W, Anal. Chem 2016, 88, 5835–5840. [PubMed: 27128102]

[16]. Tassali N, Kotera N, Boutin C, Léonce E, Boulard Y, Rousseau B, Dubost E, Taran F, Brotin T, Dutasta J-P, et al., Anal. Chem 2014, 86, 1783–1788. [PubMed: 24432871]

[17]. Riggle BA, Wang Y, Dmochowski IJ, J. Am. Chem. Soc 2015, 137, 5542–5548. [PubMed: 25848822]

[18]. Piontek A, Witte C, Rose HM, Eichner M, Protze J, Krause G, Piontek J, Schröder L, Ann. N. Y. Acad. Sci 2017, 1397, 195–208. [PubMed: 28636798]

[19]. Witte C, Martos V, Rose HM, Reinke S, Klippel S, Schröder L, Hackenberger CPR, Angew. Chemie - Int. Ed 2015, 54, 2806–2810.

[20]. Wang Y, Dmochowski IJ, Chem. Commun 2015, 51, 8982–8985.

[21]. Schnurr M, Sloniec-Myszk J, Döpfert J, Schröder L, Hennig A, Angew. Chemie - Int. Ed 2015, 54, 13444–13447.

[22]. Yang S, Yuan Y, Jiang W, Ren L, Deng H, Bouchard LS, Zhou X, Liu M, Chem. - A Eur. J 2017, 23, 7648–7652.

[23]. Zeng Q, Guo Q, Yuan Y, Yang Y, Zhang B, Ren L, Zhang X, Luo Q, Liu M, Bouchard LS, et al., Anal. Chem 2017, 89, 2288–2295. [PubMed: 28192930]

[24]. Kunth M, Lu GJ, Witte C, Shapiro MG, Schröder L, ACS Nano 2018, 12, 10939–10948. [PubMed: 30204404]

[25]. Kim BS, Ko YH, Kim Y, Lee HJ, Selvapalam N, Lee HC, Kim K, Chem. Commun 2008, 0, 2756.

[26]. Barrow SJ, Kasera S, Rowland MJ, del Barrio J, Scherman OA, Chem. Rev 2015, 115, 12320–12406. [PubMed: 26566008]

[27]. Slack CC, Finbloom JA, Jeong K, Bruns CJ, Wemmer DE, Pines A, Francis MB, Chem. Commun 2017, 53, 1076–1079.

[28]. Finbloom JA, Slack CC, Bruns CJ, Jeong K, Wemmer DE, Pines A, Francis MB, Shen C, New EJ, Major JL, et al., Chem. Commun 2016, 52, 3119–3122.

[29]. Trepper TS, Mccollum EE, De Jong P, Korman H, Gingerich W, Franklin C, Res. Comm. Solut. Focus. Br. Ther. Assoc 1997, 1, 1–16.

[30]. Shchepotina EG, Pashkina E. a., Yakushenko EV, Kozlov V. a., Nanotechnologies Russ 2011, 6, 773–779.

[31]. Jin Jeon Y, Kim S-YY, Ho Ko Y, Sakamoto S, Yamaguchi K, Kim K, Jeon YJ, Kim S-YY, Ko YH, Sakamoto S, et al., Org. Biomol. Chem 2005, 3, 2122–2125. [PubMed: 15917899]

[32]. Chen Y, Huang Z, Zhao H, Xu JF, Sun Z, Zhang X, ACS Appl. Mater. Interfaces 2017, 9, 8602–8608. [PubMed: 28194936]

[33]. Cao L, Hettiarachchi G, Briken V, Isaacs L, Angew. Chemie Int. Ed 2013, 52, 12033–12037.

[34]. Hermanson GT, (Strept)Avidin–Biotin Systems, 2013.

[35]. Isaacs L, Park S, Liu S, Ko YH, Selvapalam N, Kim Y, Kim H, Zavalij PY, Kim G, Lee H, et al., 2005, 8, 18000–18001.

[36]. Buschmann HJ, Mutihac L, Mutihac RC, Schollmeyer E, Thermochim. Acta 2005, 430, 79–82.

[37]. Danylyuk O, Fedin VP, Sashuk V, Chem. Commun 2013, 49, 1859–1861.

[38]. Freeman WA, Acta Crystallogr. Sect. B 1984, 40, 382–387.

[39]. Roose BW, Zemerov SD, Dmochowski IJ, Xenon–Protein Interactions: Characterization by X-Ray Crystallography and Hyper-CEST NMR, Elsevier Inc., 2018.

[40]. Tilton RF, Kuntz ID, Biochemistry 1982, 21, 6850–6857. [PubMed: 7159568]

[41]. Wang IJ,Roose Y, Palovcak BW, Carnevale EJ, Dmochowski V, Angew. Chem. Int. Ed. Engl 2015, 91, 165–171.

[42]. Roose BW, Zemerov SD, Dmochowski IJ, Chem. Sci 2017, 7631–7636. [PubMed: 29568427]

[43]. Sears DN, Jameson CJ, 2003, 119, DOI 10.1063/1.1625364.

[44]. Lowery TJ, Garcia S, Chavez L, Ruiz EJ, Wu T, Brotin T, Dutasta J-P, King DS, Schultz PG, Pines A, et al., ChemBioChem 2006, 7, 65–73. [PubMed: 16342304]

[45]. Sears DN, Jameson CJ, Harris RA, 2004, 120, 3277–3283.

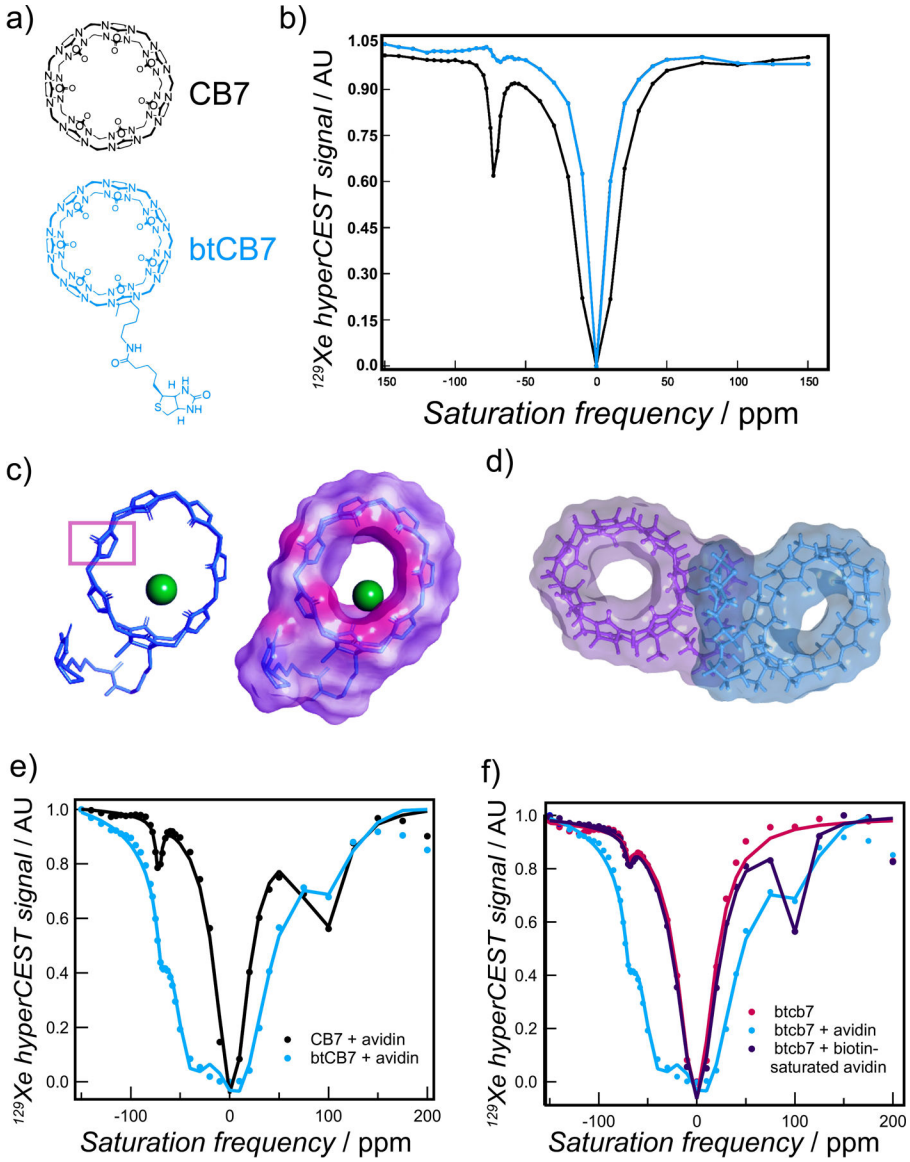

Figure 1.

a) Structures of unmodified and biotinylated (bt-)CB7. b) A ^{129}Xe hyperCEST z-spectrum shows that both structures provide a similar chemical environment for xenon at −68 ppm, but that the population of xenon in btCB7 is greatly reduced. Conformational searches followed by MD simulations of btCB7 in monomer and dimer forms indicate that c) a btCB7 with an inverted glycouril unit (ibtCB7, highlighted) may make xenon capture possible in this relatively larger CBn, but d) ibtCB7 dimer formation may restrict xenon exchange, leading to a reduced signal compared to unmodified CB7. e) Unlike unmodified CB7, ibtCB7 gives rise to a new signal at −40 ppm when avidin is introduced. f) This signal does not appear when avidin is pre-saturated with biotin, indicating that the signal at −40 ppm is from xenon in avidin-bound btCB7.

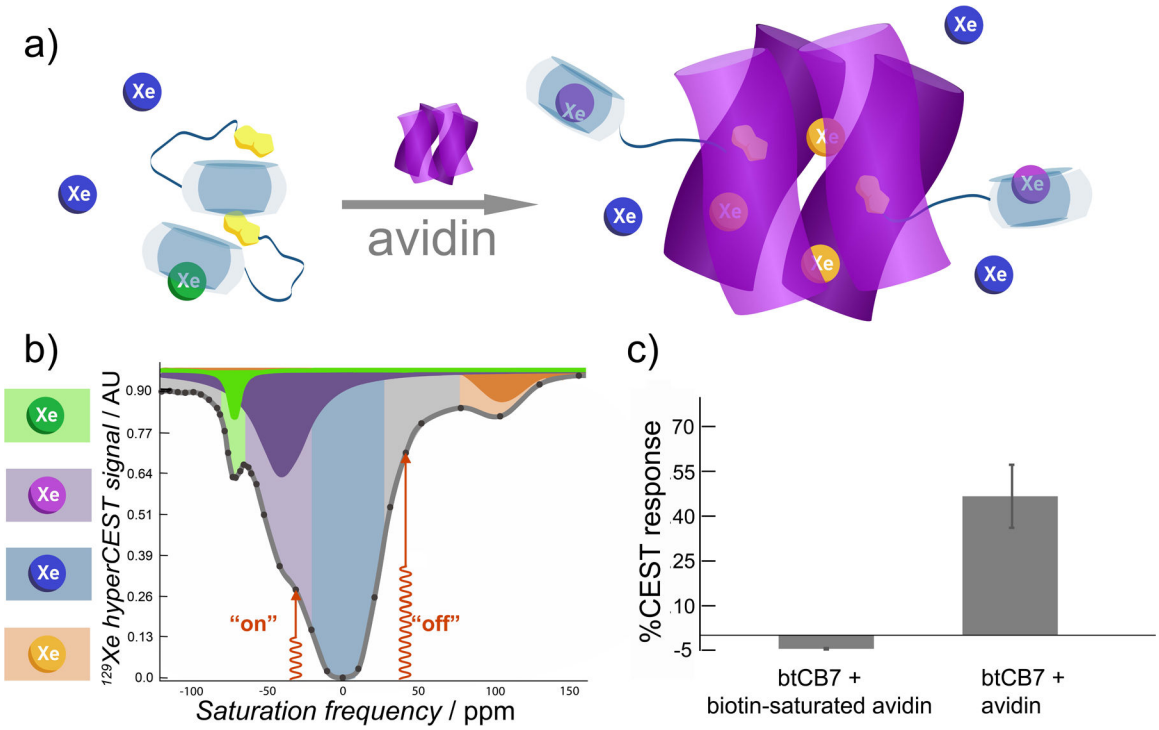

Figure 2.

a) Four distinct xenon populations in this system can be identified in b) a ^{129}Xe hyperCEST z-spectrum (1:1 ratio of 50 μM btCB7 to avidin binding sites shown). The largest population of xenon is dissolved in the solvent (blue, 0 ppm), to which the chemical shifts of all populations are referenced. Some xenon undergoes exchange with ibtCB7 (green, −68 ppm). Upon addition of avidin, btCB7 binds to the protein, leading to a response for the btCB7-avidin complex (purple, −40 ppm). Xenon also interacts directly with avidin (orange, 100 ppm). c) CEST contrast gained as a result of adding avidin is evaluated by subtracting the 'off' signal at the position equal and opposite the dissolved xenon resonance at 40 ppm from the 'on' signal at −40 ppm, corresponding to btCB7 bound to avidin.

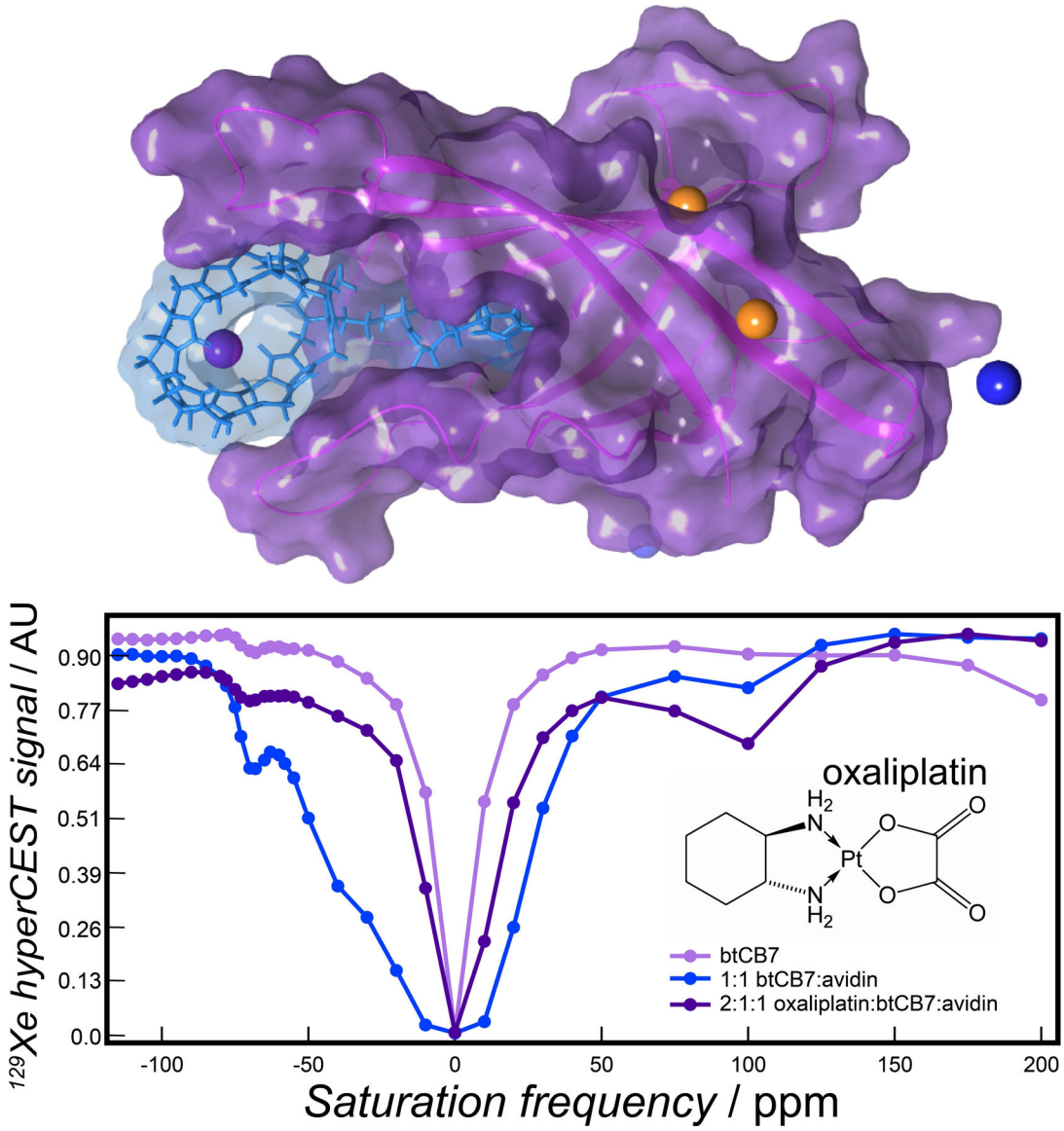

Figure 3.

Top: Docking and MD simulations show that btCB7 fits into the biotin binding pocket of monomeric avidin with the CB portion resting between the L3,4 and L7,8 loops. Xenon atoms transiently caught in hydrophobic pockets of the monomer itself were also observed. Bottom: ^{129}Xe hyperCEST spectra of 50 μM btCB7 before and after addition of 100 μM oxaliplatin in the presence of avidin. Addition of oxaliplatin results in the disappearance of the avidin-bound btCB7 response at −40 ppm, indicating that oxaliplatin blocks xenon from the avidin-bound sensor. The signal for the unbound sensor, however, is unaffected, implicating weaker binding of oxaliplatin.